Journal of Molecular Liquids 410 (2024) 125491

Contents lists available at ScienceDirect

Journal of Molecular Liquids

journal homepage: www.elsevier.com/locate/molliq

Design and synthesis of new benzoxazole derivatives and study of their interactions with a G4 model by UV spectroscopy and in silico methods

Daniela Giunta [a], Giovanni N. Roviello [b], Maurizio Solinas [a,*]

[a] Institute of Biomolecular Chemistry, National Research Council of Italy (ICB-CNR), Research Site of Sassari Traversa La Crucca 3, I-07100 Sassari, Italy
[b] Institute of Biostructures and Bioimaging, National Research Council of Italy (IBB-CNR), Area di Ricerca Site and Headquarters, Via Pietro Castellino 111, 80131 Naples, Italy

ARTICLE INFO

Keywords:
UV Spectroscopy
G-Quadruplex
Click Chemistry
Docking

ABSTRACT

In this study, we synthesized novel benzoxazol-2-ylmethyl-(1*H*-1,2,3-triazol-4-yl)phenyl)-3-aminopropanamides (**6a-d**) in high yields by means of the Copper-catalysed Azide-Alkyne Cycloaddition (CuAAC) reaction. The synthetic pathway involves the conversion of 2-aminophenol to 2-(bromomethyl)benzoxazole **1**, followed by its transformation into the azide derivative **2**. Subsequent reaction with functionalized arylalkynes **5a-d** under Sharpless's reaction conditions yields the desired compounds **6a-d**. These benzoxazoles were then evaluated as G-Quadruplex DNA (G4) ligands by UV spectroscopy studies using a telomeric sequence (Tel22) as G4 model. We studied how the absorbance at λ_{max} varies over time for the **6a-d**/Tel22 mixtures at different molar ratios. Moreover we carried out melting experiments in order to point out any possible stabilization effects arising by ligand interaction. Our findings indicate that Tel22 is slighlty but significantly stabilized by compound **6b** at a 1:1 ratio. Furthermore for **6b**, these results align well with in silico predictions suggesting that the ligand acts as groove binder interacting with six guanosine residues of the telomeric model.

1. Introduction

The nucleus of each human somatic cell contains 46 threadlike structures made of proteins and deoxyribonucleic acids (DNA), called chromosomes [1]. Chromosomes end with telomeres, a region of repetitive nucleotide sequences [2]. Telomeres protect the chromosomal DNA from progressive degradation: they are like aglets at the end of the shoelaces. The maintenance of telomeres is essential for chromosome stability and, although they do not contain significant genetic information, they play an important role in determining the lifetime of each cell. In normal cells, telomeres are constantly shortened with progressive cell division, until replicative senescence and apoptosis when they become critically small [3,4]. Structurally, telomeres are characterized by repetition of –TTAGGG– nucleotides for about 5–10 kDa. These sequences, formed by specific guanine-rich regions, have a characteristic non-canonical secondary structure known as G-quadruplex (G4) [5]. They are indeed organized in square planar arrangements (G-tetrads), held together by Hoogsteen hydrogen bondings, and stabilized by a central metal cation (Na^+ or K^+). Moreover, G-tetrads can adopt *syn* or *anti* glycosidic conformation, antiparallel, parallel and hybrid topologies as well as intra- and intermolecular forms [6]. While DNA polymerase catalyses chromosomes duplication, telomerase (a reverse transcriptase enzyme) is responsible for telomeres maintenance. Telomerase is tightly repressed in most human somatic cells, but when activated it triggers one of the mechanisms responsible for cell immortalization found in 80–85 % of all human cancers [7]. Nowadays, both telomerase and its substrate (telomeric G4) are widely considered as targets to develop new anticancer drugs. Molecules able to selectively interact with telomeric G4 structures in tumour cells may act as chemotherapeutic agents by inducing telomere shortening, cell cycle arrest, senescence and apoptosis [8]. Most of the molecules known to be able to non-covalently bind to G4 structures are composed by one or more fused aromatic rings [9]. In all cases, the aromatic systems target the guanines in the G-quartets, while one or more side chains with a protonable group are accountable for interaction with the G4′s grooves or loops [9].

Benzoxazoles, benzothiazoles and benzoselenazoles belong to a class of chemical compounds (*i.e.* benzoazoles) in which a benzene ring is fused together with a five-membered heterocycle having, beside the nitrogen, an oxygen, a sulfur or a selenium atom respectively. Specifically for benzoxazoles, nitrogen and oxygen may potentially act as

* Corresponding author at: Institute of Biomolecular Chemistry, National Research Council of Italy (ICB-CNR), Research site of Sassari Traversa La Crucca 3, I-07100 Sassari, Italy.
E-mail address: maurizio.solinas@cnr.it (M. Solinas).

https://doi.org/10.1016/j.molliq.2024.125491
Received 18 April 2024; Received in revised form 14 June 2024; Accepted 10 July 2024
Available online 16 July 2024

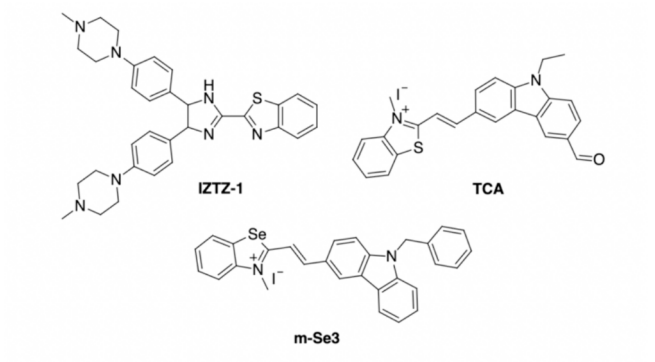

Fig. 1. Example of benzoazole G4 ligands reported in the literature.

hydrogen acceptors. Moreover, this scaffold favours either π–π stacking and hydrophobic interaction. Finally, benzoxazole is considered as the bioisostere of adenine and guanine nucleobases. Therefore, it is likely that derivatives of this molecule can target the guanines in the G4s. While few examples of molecules containing benzothiazole [10] and benzoselenazole [11] scaffolds have been reported as *c-MYC* (a G4 oncogene) transcription inhibitors (see Fig. 1), to the best of our knowledge, there are no examples of benzoxazole-based structures described as telomeric G4 ligands. Because of the mentioned structural and electronic features, together with its easy functionalization and chemical modification we believe that novel structures based on the benzoxazole core may have the potential to interact with G4s.

We hereby report our efforts in the design and synthesis of new benzoxazole derivatives, as well as the study of their interaction with a telomeric G4 model, namely Tel22 d[$AG_3(T_2AG_3)_3$], by means of UV spectroscopy. To provide a preliminary understanding of the interactions between the ligands and Tel22 at the molecular level, computational simulations using the HDOCK docking strategy are also reported [12].

2. Experimental

2.1. General information

Substrates and reagents were purchased from commercial suppliers and used without further purification. All reactions were run under a positive pressure of dry N_2 unless otherwise specified. Tel22 was annealed by heating at 95 °C for 5 min followed by cooling at RT overnight (buffer 16 mM TRIS-HCl, 50 mM NaCl). NMR spectra were recorded on a Varian Mercury (^{1}H 400 MHz, ^{13}C 101 MHz), or on a Bruker Ascend 600 (^{1}H 600 MHz, ^{13}C 151 MHz) at room temperature. Chemical shifts were described relative to the residual solvent peak in all cases and were reported in ppm with multiplicity indicated as follow: s = singlet; d = doublet; t = triplet; q = quartet; quin = quintuplet; sext = sextuplet; sept = septuplet; m = multiplet; bs = broad signal. Coupling constants (*J*) are given in Hz. UV spectra were recorded on an Agilent Cary 3500 compact Peltier using a dual-chamber quartz or a normal quartz cuvette cell. All spectroscopic experiments were run in triplicate and repeated five times. Standard deviation values for UV absorbance measurements were < 0.5%. Melting temperatures were determined as the minimum of the 1st derivative calculated for each denaturation curves. GC–MS analyses were carried out with an Agilent GC 7820A equipped with an Agilent MSD 5977E (Column: Zebron ZB-5 60 m × 0.25 mm, i.d. = 0.25 μm). HPLC/MS analyses were obtained using Agilent 1100 LC/MSD. Melting points were collected using a BÜCHI B-540 and are uncorrected. IR spectra were recorded on KBr disks using a Thermo Nicolet Avatar 330 FT-IR. Purity of compounds is > 95% as determined by elemental analysis carried out with a Thermo Scientific FlashSmart elemental analyser.

Synthesis of 2-(bromomethyl)benzo [*d*] oxazole (1). A mixture of 2–aminophenol (0.8 g, 7.3 mmol), bromoacetic acid (1.4 g, 10.1 mmol) and polyphosphoric acid (ca 15 mL) were stirred at 130 °C for 4 h. The reaction mixture was then cooled and poured into a water/DCM mixture. The organic layers were dried over anhydrous $MgSO_4$ and the solvent removed under vacuum. **1** (1.4 g, 6.6 mmol) was obtained enough pure for the following reaction as a pale-yellow oil (yield = 90%). ^{1}H and ^{13}C NMR characterization correspond to what previously described. [13] MS (*m/z*): 211.0 $[M]^+$, 213.0 $[M]^+$, 132.0 $[M–Br]^+$.

Synthesis of 2-(azidomethyl)benzo [*d*] oxazole (2). A mixture of **1** (1.0 g, 4.7 mmol) and NaN_3 (0.367 g, 5.6 mmol) in 30 mL of a 1:1 mixture of ^{t}BuOH/H_2O is heated at 50 °C overnight. Stoichiometric $AgNO_3$ (0.8 g, 4.7 mmol) is added to the mixture and the resulting precipitated AgBr is filtered off. The obtained stock solution can be directly used for the CuAAC reaction. Otherwise, to isolate the azide derivative, the volume of the reaction mixture is reduced under vacuum and compound **2** extracted with DCM. The organic phases are dried over anhydrous $MgSO_4$ and the solvent removed under vacuum to lead **2** (818 g, 4.7 mmol) in quantitative yield. ^{1}H and ^{13}C NMR and MS characterization correspond to what previously described [14].

Synthesis of 3-chloro-*N*-(4-ethynylphenyl)propanamide (3). To a mixture of 3-chloropropanoyl chloride at −10 °C (0.21 g, 1.7 mmol) in 5 mL of freshly distilled DCM, was added dropwise a cooled solution of 4-ethynylaniline (0.2 g, 1.7 mmol in 5 mL DCM). The reaction mixture was stirred for 1 h. The crude mixture was extracted with aqueous $NaHCO_3$ (0.1 N) and DCM. The organic phases are dried over anhydrous $MgSO_4$ and the solvent removed under vacuum to lead pure **3** (0.35 g, 1.7 mmol) in quantitative yield. Yellow solid, mp 144–145 °C. ^{1}H NMR (400 MHz, $CDCl_3$): δ 7.52–7.50 (m, 2H, Ar*H*), 7.47–7.45 (m, 2H, Ar*H*), 7.35 (bs, 1H, N*H*), 3.88 (t, J = 6.3 Hz, 2H, CH_2), 3.05 (s, 1H, AlkyneC*H*), 2.83 (t, J = 6.3 Hz, 2H, CH_2). ^{13}C NMR (101 MHz, $CDCl_3$) δ 180.0, 167.8, 137.9, 133.2 (2C), 119.6 (2C), 118.3, 83.3, 40.7, 39.8. IR (KBr): ν 3285, 3184, 3116, 1664, 1600 cm^{-1}. MS (EI): *m/z* 207.1 $[M]^+$, 117.1 $[C_8H_6N+H]^+$ (100). Anal. calcd for $C_{11}H_{10}ClNO$: C, 63.62; H, 4.85; N, 6.75 %. Found: C, 63.84; H, 4.87; N, 6.72 %.

2.2. General procedure for the synthesis of 3-alkylamino-propanamides (5a-d)

A cold solution (0 °C) of the appropriate amine (3.0 mmol for **4a** and **4d**; 2.0 mmol for **4b** and **4c**) in 5 ml of dry acetonitrile (ACN) was added dropwise to a mixture of 3-chloro-*N*-(4-ethynylphenyl)propanamide **3** (0.21 g, 1.0 mmol, 15 mL of ACN) at 0 °C. The reaction was then stirred at 50 °C for 24 h. The reaction was monitored by TLC analysis (hexane/ethyl acetate = 7:3). The crude mixture was extracted with aqueous $NaHCO_3$ (1 N) and DCM. The organic phases are dried over anhydrous $MgSO_4$ and the solvent removed under vacuum to lead pure propanamides **5a-d**.

3-(diethylamino)-*N*-(4-ethynylphenyl)propanamide (5a). Yellow oil, yield 98%. ^{1}H NMR (600 MHz, $CDCl_3$) δ 11.46 (s, 1H, N*H*), 7.49 (d, J = 8.6 Hz, 2H, Ar*H*), 7.42 (d, J = 8.6 Hz, 2H, Ar*H*), 3.02 (s, 1H, AlkyneC*H*), 2.78–2.73 (m, 2H, CH_2), 2.66 (q, J = 7.2 Hz, 4H, NCH_2), 2.52–2.47 (m, 2H, CH_2), 1.12 (t, J = 7.2 Hz, 6H, CH_3). ^{13}C NMR (151 MHz, $CDCl_3$) δ 171.2, 139.6, 133.1 (2C), 119.1 (2C), 116.9, 83.8, 76.4, 49.0, 46.0 (2C), 33.3, 11.6 (2C). IR (KBr): ν 3289, 2971, 1825, 1668, 1593 cm^{-1}. MS (EI): *m/z* 244.1 $[M]^+$, 215.1 $[M–CH_2CH_3]^+$. Anal. calcd for $C_{15}H_{20}N_2O$: C, 73.74; H, 8.25; N, 11.47 %. Found: C, 73.45; H, 8.28; N, 11.43 %.

***N*-(4-ethynylphenyl)-3-(pyrrolidin-1-yl)propanamide (5b).** Light yellow solid, yield 97%, mp 50–52 °C. ^{1}H NMR (400 MHz, $CDCl_3$) δ 11.46 (s, 1H, N*H*), 7.46 – 7.41 (m, 4H, Ar*H*), 3.03 (s, 1H, AlkyneC*H*), 2.85 – 2.82 (m, 2H, CH_2), 2.67 (bs, 4H, NCH_2), 2.54 – 2.51 (m, 2H, CH_2), 1.90 (bs, 4H, –CH_2CH_2–). ^{13}C NMR (101 MHz, $CDCl_3$) δ 171.2, 139.6, 133.0 (2C), 119.3 (2C), 116.9, 83.8, 76.5, 53.2 (2C), 51.3, 34.7, 23.8 (2C). IR (KBr): ν 3233, 1672, 1596 cm^{-1}. MS (EI): *m/z* 242.2 $[M]^+$,

117.1 $[C_8H_6N+H]^+$. Anal. calcd for $C_{15}H_{18}N_2O$: C, 74.35; H, 7.49; N, 11.56 %. Found: C, 74.63; H, 7.46; N, 11.60 %.

***N*-(4-ethynylphenyl)-3-(piperidin-1-yl)propanamide (5c).** Yellow powder, yield 96%, mp 107–108 °C. ^{1}H NMR (400 MHz, $CDCl_3$) δ 11.50 (s, 1H, N*H*), 7.51 – 7.54 (m, 2H, Ar*H*), 7.45 – 7.41 (m, 2H, Ar*H*), 3.03 (s, 1H, AlkyneC*H*), 2.72 – 2.69 (m, 2H, CH_2), 2.60 (bs, 4H, Cy*H*) overlapped with 2.56 –2.53 (m, 2H, CH_2), 1.74 – 1.69 (m, 6H, Cy*H*). ^{13}C NMR (101 MHz, $CDCl_3$) δ 171.1, 139.6, 133.0 (2C), 119.1 (2C), 116.8, 83.8, 76.4, 54.3, 53.7 (2C), 32.6, 26.4 (2C), 24.3. IR (KBr): ν 3277, 2938, 1676, 1597 cm^{-1}. MS (EI): *m/z* 256.1 $[M]^+$. Anal. calcd for $C_{16}H_{20}N_2O$: C, 74.97; H, 7.86; N, 10.93 %. Found: C, 75.26; H, 7.82; N, 10.89 %.

***N*-(4-ethynylphenyl)-3-morpholinopropanamide (5d).** White solid, yield 99%, mp 134–136 °C. ^{1}H NMR (600 MHz, $CDCl_3$) δ 10.91 (s, 1H, N*H*), 7.52 – 7.48 (m, 2H, Ar*H*), 7.47 – 7.42 (m, 2H, Ar*H*), 3.83 (bs, 4H, CH_2), 3.04 (s, 1H, AlkyneC*H*), 2.74 (t, J = 6.6 Hz, 2H, CH_2), 2.63 (bs, 4H, CH_2), 2.55 (t, J = 6.6 Hz, 2H, CH_2). ^{13}C NMR (151 MHz, $CDCl_3$) δ 170.5, 139.2, 133.1 (2C), 119.2 (2C), 117.2, 83.6, 76.7, 67.2 (2C), 54.2, 52.9 (2C), 32.3. IR (KBr): ν 3354, 3200, 2955, 1669, 1517 cm^{-1}. MS (EI): *m/z* 258.1 $[M]^+$. Anal. calcd for $C_{15}H_{18}N_2O_2$: C, 69.74; H, 7.02; N, 10.84 %. Found: C, 69.97; H, 7.04; N, 10.79 %.

2.3. General procedure for the synthesis of compounds (6a-d)

To a mixture of 2-(azidomethyl)benzo[*d*]oxazole **2** (0.2 g, 1.2 mmol) and NaAsc (0.2 g, 1.0 mmol) in a solution of ^{t}BuOH/H_2O (30 mL, 1:1), $Cu(OAc)_2{\cdot}H_2O$ (0.024 g, 0.12 mmol) was added before addition of the proper *N*-(4-ethynylphenyl)-3-alkylamino-propanamide **5a-d** (1.2 mmol). The reaction mixture was stirred at RT overnight. ^{t}BuOH was removed under vacuum and the aqueous phase extracted with DCM. Finally, the organic phases were washed with EDTA 1 N, dried over $MgSO_4$ and the solvent removed under high vacuum to yield pure **6a-d**.

***N*-(4-(1-(benzo[*d*]oxazol-2-ylmethyl)-1*H*-1,2,3-triazol-4-yl) phenyl)-3-(diethylamino)propanamide (6a).** Light orange solid, yield > 99%, mp 114–116 °C. ^{1}H NMR (600 MHz, $CDCl_3$) δ 11.37 (s, 1H, N*H*), 7.97 (s, 1H, Trz*H*), 7.79–7.71 (d, J = 8.6 Hz, 2H, Ar*H* overlapped with m, 1H, Ar*H*), 7.59 (d, J = 8.6 Hz, 2H, Ar*H*), 7.40–7.51 (m, 1H, Ar*H*), 7.40–7.34 (m, 2H, Ar*H*), 5.87 (s, 2H, TrzCH_2Bzx), 2.78 (t, J = 5.9 Hz, 2H, CH_2), 2.68 (q, J = 7.2 Hz, 4H, CH_2), 2.51 (t, J = 5.9 Hz, 2H, CH_2), 1.13 (t, J = 7.2 Hz, 6H, CH_3). ^{13}C NMR (151 MHz, $CDCl_3$) δ 171.0, 158.8, 151.1, 148.5, 140.8, 139.1, 126.6 (2C), 126.2, 125.5, 125.1, 120.7, 119.9, 119.7 (2C), 111.1, 49.0, 47.3, 46.0 (2C), 33.2, 11.5 (2C). IR (KBr): ν 3101, 2966, 2816, 1670, 1598 cm^{-1}. MS (ESI): *m/z* 419.2 $[M+H]^+$. Anal. calcd for $C_{23}H_{26}N_6O_2$: C, 66.01; H, 6.26; N, 20.08 %. Found: C, 66.24; H, 6.23; N, 20.15 %.

***N*-(4-(1-(benzo[*d*]oxazol-2-ylmethyl)-1*H*-1,2,3-triazol-4-yl) phenyl)-3-(pyrrolidin-1-yl)propanamide (6b).** Light brown solid, yield 70%, mp 142–144 °C. ^{1}H NMR (400 MHz, $CDCl_3$) δ 11.36 (s, 1H, N*H*), 7.97 (s, 1H, Trz*H*), 7.80–7.70 (m, 3H, Ar*H*), 7.59–7.49 (m, 3H, Ar*H*), 7.44–7.33 (m, 2H, Ar*H*), 5.89 (s, 2H, TrzCH_2Bzx), 2.86 (dd, J = 6.8, 4.9 Hz, 2H, CH_2), 2.69 (bs, 4H, CH_2), 2.55 (dd, J = 6.8, 4.9 Hz, 2H, CH_2), 1.91 (bs, 4H, CH_2). ^{13}C NMR (101 MHz, $CDCl_3$) δ 170.0, 158.8, 151.2, 148.5, 140.8, 138.9, 126.6 (2C), 126.3, 125.8, 125.2, 120.7, 120.0 (2C), 119.9, 111.2, 53.7 (2C), 51.6, 47.4, 34.5, 23.8 (2C). IR (KBr): ν 3338, 3095, 2962, 2797, 1661, 1594 cm^{-1}. MS (ESI): *m/z* 417.1 $[M+H]^+$. Anal. calcd for $C_{23}H_{24}N_6O_2$: C, 66.33; H, 5.81; N, 20.18 %. Found: C, 66.59; H, 5.78; N, 20.26 %.

***N*-(4-(1-(benzo[*d*]oxazol-2-ylmethyl)-1*H*-1,2,3-triazol-4-yl) phenyl)-3-(piperidin-1-yl)propanamide (6c).** Light brown solid, yield 70%, mp 165–168 °C. ^{1}H NMR (400 MHz, $CDCl_3$) δ 11.52 (s, 1H, N*H*), 7.98 (s, 1H, Trz*H*), 7.80–7.73 (d, J = 9.0 Hz, 2H, Ar*H* overlapped with m, 1H, Ar*H*), 7.61 (d, J = 9.0 Hz, 2H, Ar*H*), 7.56–7.52 (m, 1H, Ar*H*), 7.43–7.35 (m, 2H, Ar*H*), 5.89 (s, 2H, TrzCH_2Bzx), 2.68–2.65 (m, 2H, Cy*H*), 2.61–2.50 (bs, 2H, CH_2 overlapped with m, 4H, Cy*H*), 1.74–1.68 (m, 6H, Cy*H*). ^{13}C NMR (101 MHz, $CDCl_3$) δ 171.0, 158.8, 151.2, 148.6, 140.8, 139.3, 126.7 (2C), 126.3, 125.6, 125.2, 120.8, 119.8, 119.8 (2C), 111.2, 54.5, 53.8 (2C), 47.4, 32.7, 26.4 (2C), 24.4. IR (KBr): ν 3344, 3083, 2928, 1664, 1592 cm^{-1}. MS (ESI): *m/z* 431.1 $[M+H]^+$. Anal. calcd for $C_{24}H_{26}N_6O_2$: C, 66.96; H, 6.09; N, 19.52 %. Found: C, 66.69; H, 6.07; N, 19.45 %.

***N*-(4-(1-(benzo[*d*]oxazol-2-ylmethyl)-1*H*-1,2,3-triazol-4-yl) phenyl)-3-morpholinopropanamide (6d).** off-white solid, yield 78%, mp 174–176 °C. ^{1}H NMR (400 MHz, $CDCl_3$) δ 10.90 (s, 1H, N*H*), 7.98 (s, 1H, Trz*H*), 7.80 (d, J = 8.8 Hz, 2H, Ar*H*), 7.78–7.74 (m, 1H, Ar*H*), 7.60 (d, J = 8.8 Hz, 2H, Ar*H*), 7.57–7.53 (m, 1H, Ar*H*), 7.43–7.36 (m, 2H, Ar*H*), 5.89 (s, 2H, TrzCH_2Bzx), 3.84 (t, J = 4.8 Hz, 4H), 2.77–2.74 (m, 2H, CH_2), 2.64 (bs, 4H, CH_2), 2.57–2.54 (m, 2H, CH_2). ^{13}C NMR (101 MHz, DMSO) δ 170.2, 160.4, 150.4, 146.7, 140.3, 139.1, 125.8, 125.7 (2C), 125.1, 124.9, 121.9, 120.0, 119.3 (2C), 111.1, 66.2 (2C), 54.1, 53.0 (2C), 46.7, 33.9. IR (KBr): ν 3309, 2945, 2842, 1655, 1591 cm^{-1}. MS (ESI): *m/z* 433.2 $[M+H]^+$. Anal. calcd for $C_{23}H_{24}N_6O_3$: C, 63.88; H, 5.59; N, 19.43 %. Found: C, 63.65; H, 5.60; N, 19.50 %.

2.4. UV–Vis studies

The UV binding experiments were performed in a quartz cuvette with two partially separated chambers (b = 2 × 4.375 mm, Hellma® Analytics). The UV interaction studies were performed by measuring first the *sum* spectrum of the two solutions in the separated chambers. Subsequently, by turning up and down the cuvette, the spectrum obtained after mixing the solutions (*mix*) was registered at different times. The UV melting experiments were performed within a temperature range of 20–90 °C using a quartz cuvette with an optical path length of 10 mm. Data were collected with a data pitch of 1 nm with a temperature rise of 1 °C/min at 295 nm. Melting temperature (Tm) values were determined as the temperatures relative to minima of the 1st derivative plots of denaturation curves. All UV experiments were repeated at least in triplicate. The buffer used in all experiments was 16 mM TRIS-HCl, 50 mM NaCl, pH = 7.6 at 25 °C.

2.5. Computational studies

The model of Tel22 used in our simulations corresponded to the structure $d[AG_3(T_2AG_3)_3]$ (PDB ID: 143D) [15] and was visualized by Discovery Studio (DS) 2021 software (Accelrys, USA) [16]. The complex predictions were obtained by docking **6a-d** ligands with the target DNA using the software HDOCK [17] with default parameters. The structures of the ligands were obtained using the MolView program (Netherlands, v2.4), which, after energy minimization, allowed us to generate three-dimensional models visualized as .pdb files by DS. The HDOCK program useful for both macromolecule-macromolecule and small molecule-macromolecule dockings [12,17,18], employed for the blind dockings described in this work, utilizes the iterative knowledge-based scoring function ITScore-PP to rank the top-10 poses obtained after the docking runs. The HDOCK score provided by the program is an energy score represented as dimensionless values: larger negative values indicate stronger binding interactions between the macromolecules. This has been reported to correlate well with experimental binding affinities [19]. The top-ranked pose (Top-1) and the Top-1–3 poses for **6a-d**/Tel22 complexes predicted by HDOCK program are considered.

3. Results and discussion

3.1. Design and synthetic procedures

A literature survey on G4 ligands indicates that several interacting ligands, such as Braco-19 and Telomestatin, have intriguing *in vivo* activities [20]. All information gained from molecular modelling, crystallographic and NMR data analysis highlight the structural features to be held in mind in the design and optimization of G4 binders. As mentioned, interaction with G4 structures occurs *via* the binding of a flat aromatic core of the ligand, establishing π-π stacking with the G-tetrads. Besides, the presence of one or more basic functionalities (often

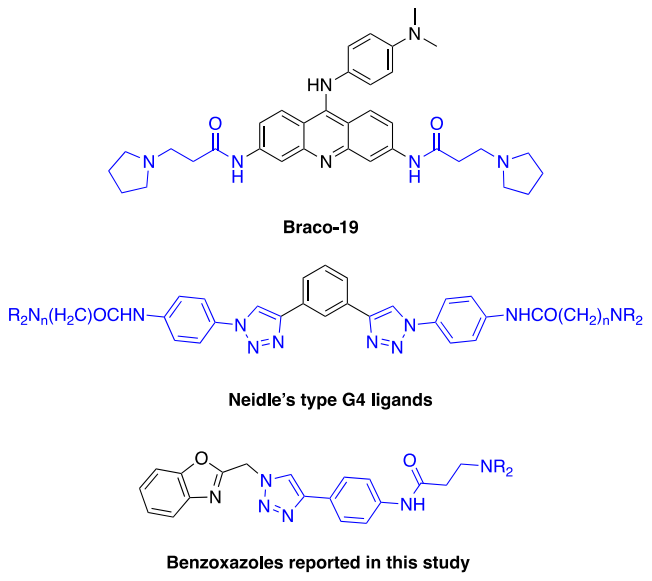

Fig. 2. Structural similarities between the 3-(amino)-*N*-(4-aryl)propanamide groups exploited as side chains in the present study and the side chains in Braco-19 and in Neidle's type G4 ligands (R = alkyl groups).

protonated at physiological pH) may be responsible for stabilization *via* interactions with the quadruplex's groves or loops [9]. Accordingly, we designed a convergent synthesis of new benzoxazole derivatives taking advantage of the Copper-catalysed Azide-Alkyne Cycloaddition (CuAAC) reaction to link 3-(amino)-*N*-(4-aryl)propanamide groups which resemble the side chains in Braco-19 and of Neidle's G4 ligands (see Fig. 2) [21].

The resulting benzoxazol-2-ylmethyl-(1*H*-1,2,3-triazol-4-yl)phenyl)-3-aminopropanamides **6a-d** are reported in Scheme 1 (see experimental section for details).

The synthetic procedures start with the dehydration of the product obtained from the reaction between 2-aminophenol and α-bromoacetic acid, by polyphosphoric acid (PPA). The reaction is carried out at 130 °C for 4 h and the product (bromomethyl)benzoxazole **1** is isolated, after extraction with organic solvent, obtaining > 99% yields. The (bromomethyl)benzoxazole **1** is then quantitatively converted into its azide derivate **2** by reaction with NaN_3 in a mixture of ^{t}BuOH/H_2O at 50 °C. The intermediate azide **2** can be isolated by extraction with organic solvents after thoughtful elimination of ^{t}BuOH. Alternatively, it is possible to store stock solutions of the 2-(azidomethyl)benzoxazole **2** after addition of stoichiometric amount of $AgNO_3$, followed by proper filtration of the resulting AgBr salt. This is necessary to remove any traces of bromide anion, as it would be detrimental in the *click*-chemistry final step [22]. To synthetise the protonable side chain, 3-chloropropionyl chloride is reacted with 4-ethynylaniline in freshly distilled dichloromethane at −10 °C (1 h) yielding 3-chloro-*N*-(4-ethynylphenyl)propanamide **3** after aqueous/organic work-up (> 99%). Compound **3** is then reacted with a two (**4c**, **4b**) or three (**4a**, **4d**) fold excess of the proper primary amine under similar reaction conditions (see Scheme 1). More in details, reactions are carried out in acetonitrile at 50 °C for 24 h. Isolated yield values are between 95% and > 99%.

Finally, the 2-(azidomethyl)benzoxazole **2** was "clicked" with each of the functionalized arylalkynes **5a-d** under Sharpless's reaction conditions ($Cu(OAc)_2{\cdot}H_2O$, NaAsc, ^{t}BuOH/H_2O, RT) [23]. Compared to the simple azide-alkyne Huisgen 1,3-dipolar cycloaddition, which requires elevated temperature and results in a mixture of 1,4 and 1,5 regioisomers, the copper catalysed version (CuAAC) is regioselective, easily carried out and has an enormous scope. Accordingly, compounds **6a-d** were obtained in > 99%, 70%, 70%, and 78% yields respectively. Get rid of the catalytic copper at the end of each *click*-chemistry steps is possible by extraction of the organic layers with aqueous EDTA until colourless solutions are obtained [24]. Subsequent drying of the organic phases leads to pure solid compounds in all cases. Noteworthy, all intermediates and final compounds are obtained as pure products in high yields and without the need for tedious chromatographic purification steps.

3.2. UV studies

UV spectroscopy is a broadly used method to follow DNA folding and unfolding transition in solution. Modifications in the oligonucleotide secondary structure determine a measurable absorbance (abs) variation mainly at its λ_{max} [25]. As peculiar feature of G-quadruplex structures, the guanines assembly forming stacked G-quartets is also accompanied by an increase in absorbance at 295 nm, therefore determining a G4′s specific denaturation profile. Thermal denaturation experiments reveal G4′s melting temperature (Tm) and provide information about its stability in a specific buffer solution. The comparison between the Tm values measured for a nucleotide in the presence and in the absence of a ligand gives evidence of the effect of the latter on the G4′s structure. Changes in the absorption profile (hyper- or hypochromism, red or blue shift) measured by UV spectroscopy result from variations in the π/π^* transition energy, due to the interaction of the orbitals of the nucleotide bases and the ligand. Nevertheless, even small alterations measured in the UV spectra could be due to a groove- or outside-binder [26]. All benzoxazoles under investigation in the present study show similar UV spectra with a maximum absorbance at approximately 267 nm, which overlap with the one measured for Tel22 at the same conditions (λ_{max} = 256 nm, see experimental section for details). Using a double chamber cell, we measured the UV spectra of the sum of each compound **6a-d** and Tel22 (in 16 mM TRIS-HCl, 50 mM NaCl buffer) and compared them with the ones obtained immediately after mixing the solutions, after 24 and 48 h [27]. For comparison, the same experiments have been also carried out with Braco-19, as it is a well-known telomeric binding ligand [28]. Generally speaking, ligands that intercalate DNA, *e.g.* Braco-19, usually causes hypochromism and bathochromism (red shift). On the other side, in case of electrostatic attraction between compounds and DNA, a certain level of hyperchromic effect is observed. This reflect

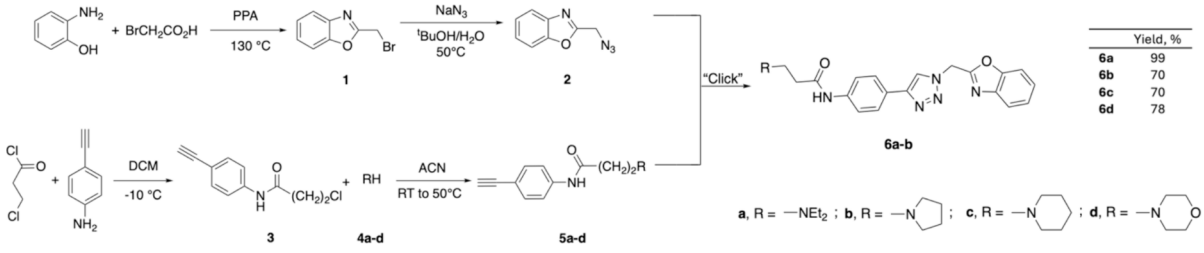

Scheme 1. Synthesis of the benzoxazole derivatives reported in the present study.

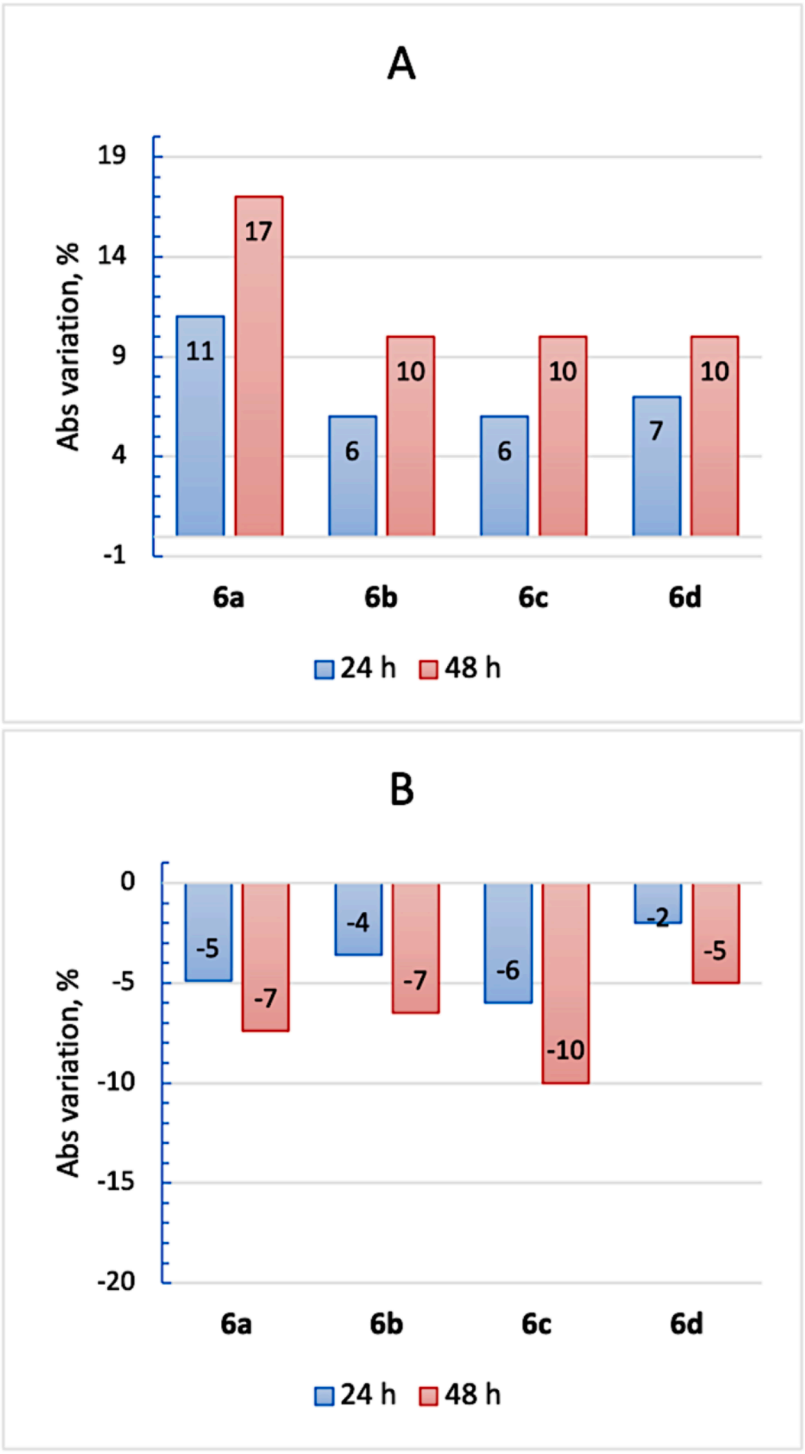

Fig. 3. Effect of added ligands **6a-d** with Tel22 as function of time: **A** = ligands/Tel22 in 1:1 molar ratio; **B** ligands/Tel22 in 20:1 molar ratio.

changes in DNA conformation and structure caused by ligand interaction [29]. Given a ligand/Tel22 molar ratio equal to 1 (1.6 μM), after 48 h, we measured for all molecules (**6a-d**) at 257 nm an hyperchromic effect which lies in the range of 10–17 % (see Fig. 3A). At the same conditions Braco-19 showed a small hypochromic effect in the range of 4 % (data not included in Fig. 3A).

In consecutive experiments, by increasing the molar ratio **6a-d**/Tel22 to 20, we observed a different behaviour. Thus, all ligands tested showed a hypochromic effect at 264 nm in the range of 2–6 % after 24 h and between 5 and 10 % after 48 h (see Fig. 3**B**). Since in previous experiments we observed that the absorbance of **6a-d** measured at λ_{max} increases linearly with the concentration (between 0.5 and 32 μM), suggesting the presence of single absorbing species, it is likely that a different type of interaction with Tel22 occur at higher ligand/Tel22

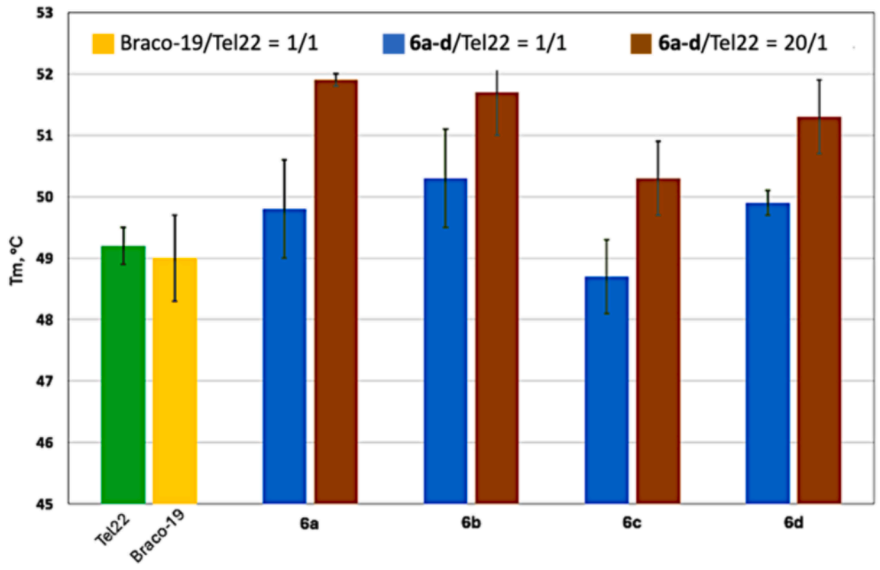

Fig. 4. Melting temperatures of mixed **6a-d**/Tel22 (1:1 and 20:1 ratios) and Braco-19/Tel22 (1:1 ratio) with relative standard deviation error bars.

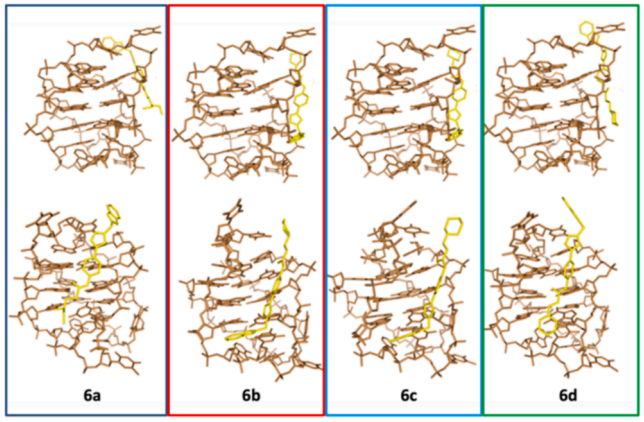

Fig. 5. Two views of each model obtained for the top-ranked complexes of **6a-d** with Tel22. G4 DNA is represented in brown, while the ligands are displayed in yellow colour for clarity.

molar ratios. In conclusion, our findings with the sum/mix UV experiments give evidence of interaction between compounds **6a-d** and Tel22.

As mentioned, Tm values of quadruplex DNA give further insight about any possible stabilization effect due to ligand interaction. We measured Tm values of the mixtures **6a-d**/Tel22 at 1:1 and 20:1 molar ratio by following denaturation curves at 295 nm. Results are reported in Fig. 4 and in Table S1. As shown, at our conditions Tel22 has a Tm of 49.2 ± 0.3 °C. Surprisingly, although Braco-19 is a well-known telomeric ligand, capable of classical intercalating binding mode, in our hands, its presence in a 1:1 ligand:DNA ratio does not cause a significant variation in the melting temperature (Tm = 49.0 ± 0.7 °C). On the contrary, when mixed at the same molar ratio with Tel22, ligands **6b** and **6d** can induce slight but significant Tm variations (ΔTm = 1.1 °C for **6b** and ΔTm = 0.7 °C for **6d**). Notably, G4 thermal stability is not the only aspect to be considered when investigating new G4 ligands. Our findings indicate that some of our derivatives not only produce UV changes in DNA binding assays, like those observed for established G4 ligands (*e.g.* Braco-19), but also enhance the thermal stability (Tm) of G4 systems. Moreover, at higher ligand concentrations (20:1) all molecules show a greater stabilization effect (1.1 < ΔTm < 2.7 °C), being compounds **6a** and **6b** the more effective (Tm 51.9 ± 0.1 °C for **6a** and Tm 51.7 ± 0.7 °C for **6b**).

Once again, this behaviour highlights a different interaction mechanism with Tel22 at higher ligand concentrations. Probably each G4 molecule can interact with more than one ligand simultaneously. Molecular docking analysis seem to confirm this behaviour for compounds **6a-d** (Fig. S5). However, at a 1:1 ratio, we obtain the most reliable results in terms of the effects of discrete ligands on the DNA quadruplex. Finally, our UV experiments evidence that **6a-d** may not only act as G4 ligands but also shows a thermal stabilizing effect (particularly for **6b** in a 1:1 ratio) thus encouraging further research in the field.

Table 1
HDOCK scores for the top ranked pose and means of the scores relative to the top-3 poses for the docking of **6a-d** with tel22. The interface DNA residues within 5.0 Å from the G4 ligand in the top-1 complexes are reported in the last column. Note how all the ligands bind similar regions of Tel22 involving five common deoxynucleotides (dG2; dG3; dG9; dG10; dT12).

Ligand	Score (pose 1)	Mean Score (pose 1–3) ± SD	Residues involved in the binding
6a	−106.79	−105.85 ± 0.83	dG2; dG3; dG9; dG10; dT12
6b	−115.30	−111.70 ± 3.13	dG2; dG3; dG4; dT5; dT6; dA7; dG8; dG9; dG10; dT12
6c	−118.68	−114.89 ± 3.40	dG2; dG3; dG4; dT5; dT6; dA7; dG8; dG9; dG10; dT12
6d	−114.18	−113.22 ± 1.28	dG2; dG3; dG4; dT5; dG9; dG10; dT11; dT12

3.3. *In silico studies*

Docking between the four compounds and the quadruplex model of the telomeric Tel22 in Na^+ (PDB ID 143D) has been conducted, as illustrated in Fig. 5. In agreement with these experiments, it has been observed that all ligands **6a-d** are predicted to function as groove binders. This ability, previously described for other bioactive molecules interacting with G-quadruplexes, is accountable for selectivity over DNA

structures [30]. Remarkably, computational studies, including molecular docking and molecular dynamics, are highly significant in the study of various nucleobase-containing systems, not just G-quadruplex structures [31,32] as evidenced by the extensive number of examples in the literature [33,34].

For all benzoxazoles the scores obtained from the HDOCK docking program are negative, thus indicating that the binding process is favoured in any case. However, based on the scores of the top-ranked pose, among ligands **6a-d**, **6c** is predicted to bind most efficaciously to Tel22 target (−118.68, Table 1). Furthermore, when considering the mean scores (pose1–3), the same molecule (**6c**) demonstrates the most favourable binding (−114.89 ± 3.40). Similar trends are observed for ligands **6b** and **6d**. On the other hand, a less efficacious interaction with G4 Tel22 is predicted for **6a** (Table 1). The conserved deoxyribonucleotide residues involved in the binding process across the ligands include dG2, dG3, dG9, dG10 and dT12. The key takeaway from the docking results is that binding involves high numbers of guanosine residues (at least 4 or in some cases even 6 as for **6b** and **6c**) which is clearly crucial for quadruplex's properties.

Thus, differently from Braco-19, a well-known intercalating binder for G4, ligands **6a-d** are groove binders, as evidenced by the docking results corresponding to the structures herein displayed with energetically favoured negative scores.

4. Conclusions

Within a research program aimed at discovering new ligands able to interact with G4 structures, we synthesized and characterized a series of new molecules based on a benzoxazole core. We have exploited the CuAAC reaction to link 3-(amino)-*N*-(4-aryl)propanamide groups, to yield benzoxazol-2-ylmethyl-(1*H*-1,2,3-triazol-4-yl)phenyl)-3-amino-propan-amides **6a-d** with high yields and without requiring tedious chromatographic purification steps. Compounds **6a-d** were tested as possible G4 ligands using the telomeric quadruplex-forming DNA model Tel22. Our study reveals that Tel22 is slightly but significantly stabilized by compound **6b** when considering a 1:1 ratio (Tm = 50.3 ± 0.8 °C; ΔTm = 1.1 °C). Moreover, UV studies indicate a certain grade of interaction between **6a-d** and Tel22 and a greater stabilization effect at higher concentration of ligands. We speculate that this effect may be due to the quadruplex interacting with more molecules rather than with a single ligand. The experimental stabilizing effect of **6b** on the quadruplex structure aligns well with the predicted interaction observed in silico. Docking of this ligand with the DNA target revealed up to six interactions with guanosine residues. Currently, we are actively engaged in the design, synthesis, and characterization of novel molecules with the goal of creating groove binders that exhibit partial stacking effects on quadruplex DNA.

CRediT authorship contribution statement

Daniela Giunta: Writing – original draft, Investigation, Data curation, Conceptualization. **Giovanni N. Roviello:** Conceptualization, Investigation - data analysis and in silico studies, Writing - original draft. **Maurizio Solinas:** Writing – original draft, Supervision, Funding acquisition, Conceptualization.

Declaration of competing interest

The authors declare that they have no known competing financial interests or personal relationships that could have appeared to influence the work reported in this paper.

Data availability

All data supporting our findings are reported in the article draft and in the supporting information.

Acknowledgements

This work has been partially funded by *European union – Next Generation EU,* PRIN PNRR project n° *P2022PZ8JE*.

Appendix A. Supplementary material

Supplementary data to this article can be found online at https://doi.org/10.1016/j.molliq.2024.125491.

References

[1] B. Alberts, R. Heald, D. Morgan, M. Raff, K. Roberts, P. Walter, Molecular Biology of the Cell (2022). W.W. Norton Co Eds.
[2] V.A. Zakian, Exp. Cell Res. 318 (2012) 1456.
[3] W. Lu, Y. Zhang, D. Liu, Z. Songyang, M. Wan, Exp. Cell Res. 319 (2013) 133.
[4] C.W. Greider, E.H. Blackburn, Cell 43 (1985) 405.
[5] J.R. Williamson, M.K. Raghuraman, T.R. Cech, Cell 59 (1989) 871.
[6] (a) J. Choi, T. Majima, Chem. Soc. Rev. 40 (2011) 5893;
(b) Y. Ma, K. Iida, K. Nagasawa, Biochem. Biophys. Res. Commun. 531 (2020) 3.
[7] (a) M. Ruden, N. Puri, Cancer Treat. Rev. 39 (2013) 444;
(b) R.R. Reddel, Curr. Pharm. Des. 20 (2014) 6361;
(c) G.M. Arndt, K.L. MacKenzie, Nat. Rev. Cancer 16 (2016) 508.
[8] (a) S. Neidle, J. Med. Chem. 59 (2016) 5987;
(b) S. Neidle, Nat. Rev. Chem. 1 (2017) 0041;
(c) S. Asamitsu, S. Obata, Z. Yu, T. Bando, H. Sugiyama, Molecules 24 (2019) 429;
(d) J. Carvalho, J.L. Mergny, G.F. Salgado, J.A. Queiroz, C. Cruz, Trends Mol. Med. 26 (2020) 849;
(e) N. Kosiol, S. Juranek, P. Brossart, A. Heine, K. Paeschke, Mol. Cancer 20 (2021) 40.
[9] A.R. Duarte, E. Cadoni, A.S. Ressurreição, R. Moreira, A. Paulo, ChemMedChem 13 (2018) 869.
[10] (a) T.-Y. Wu, Q. Huang, Z.-S. Huang, M.-H. Hu, J.-H. Tan, Bioorg. Chem. 99 (2020) 103866;
(b) Y. Venkata Suseela, P. Sengupta, T. Roychowdhury, S. Panda, S. Talukdar, S. Chattopadhyay, S. Chatterjee, T. Govindaraju, ACS Bio. Med. Chem. Au. 2 (2022) 125.
[11] T.-Y. Wu, X.-C. Chen, G.-X. Tang, W. Shao, Z.-C. Li, S.-B. Chen, Z.-S. Huang, J.-H. Tan, J. Med. Chem. 66 (2023) 5484.
[12] Majumder, S.K. Mondal, S. Mukhoty, S. Bag, A. Mondal, Y. Begum, K. Sharma, A. Banik, Food Chem. 13 (2022) 100212.
[13] A.M.S. Soares, S.P.G. Costa, M.S.T. Gonçalves, Tetrahedron 66 (2010) 8189.
[14] W.L. Heaner IV, C.S. Gelbaum, L. Gelbaum, P. Pollet, K.W. Richman, W. DuBay, J. D. Butler, G. Wells, C.L. Liotta, RSC Adv. 3 (2013) 13232.
[15] Y. Wang, D.J. Patel, Structure 1 (1993) 263.
[16] S.S. Pawar, S.H. Rohane, Asian J. Res. Chem. 14 (2021) 86.
[17] (a) Y. Yan, D. Zhang, P. Zhou, B. Li, S.-Y. Huang, Nucl. Acids Res. 45 (2017) W365;
(b) Y. Yan, H. Tao, J. He, S.-Y. Huang, Nat. Protoc. 15 (2020) 1829.
[18] F. Greco, A.P. Falanga, M. Terracciano, C. D'Ambrosio, G. Piccialli, G. Oliviero, G. N. Roviello, N. Borbone, Biomol. 12 (2022) 1071.
[19] S.-Y. Huang, X. Zou, Proteins 72 (2008) 557.
[20] (a) A.M. Burger, F. Dai, C.M. Schultes, A.P. Reszka, M.J. Moore, J.A. Double, S. Neidle, Cancer Res. 65 (2005) 1489;
(b) T. Tauchi, K. Shin-Ya, G. Sashida, M. Sumi, S. Okabe, J.H. Ohyashiki, K. Ohyashiki, Oncogene 25 (2006) 5719.
[21] A.D. Moorhouse, A.M. Santos, M. Gunaratnam, M. Moore, S. Neidle, J.E. Moses, J Am Chem Soc 128 (2006) 15972.
[22] R.M. Moorman, M.B. Collier, B.H. Frohock, M.D. Womble, J.M. Chalker, Org. Biomol. Chem. 13 (2015) 1974.
[23] V.V. Rostovtsev, L.G. Green, V.V. Fokin, K.B. Sharpless, Angew. Chem. Int. Ed. 41 (2002) 2596.
[24] D. Giunta, A. Arras, P. Peluso, M. Solinas, Results Chem. 3 (2021) 100122.
[25] (a) J.L. Mergny, L. Lacroix, Curr. Protoc. Nucleic Acid Chem. (2009) unit 17.1.1;
(b) Olsen, L.A. Marky, G-Quadruplex DNA, Methods Mol. Biol. 608 (2010), 147 P. Baumann eds;
(c) F. Zarrilli, F. Amato, C.M. Morgillo, B. Pinto, G. Santarpia, N. Borbone, S. D'Errico, B. Catalanotti, G. Picciallli, G. Castaldo, G. Oliviero, Molecules 22 (2017) 1144.
[26] (a) Y. Sun, F. Ji, R. Liu, J. Lin, Q. Xu, C. Gao, J. Lumin. 132 (2012) 507;
(b) S. Bhattacharjee, P.K. Sengupta, S. Bhowmik, RSC Adv 7 (2017) 37230.
[27] C. Riccardi, D. Capasso, G.M. Rozza, C. Platella, D. Montesarchio, S. Di Gaetano, T. Marzo, A. Pratesi, L. Messori, G.N. Roviello, D. Musumeci, J. Inorg. Biochem. 203 (2020) 110868.
[28] N.H. Campbell, G.N. Parkinson, A.P. Reszka, S. Neidle, J. Am. Chem. Soc. 130 (2008) 6722.
[29] M. Sirajuddin, S. Ali, A. Badshah, J. Photochem. Photobiol. B 124 (2013) 1.
[30] S. Cosconati, L. Marinelli, R. Trotta, A. Virno, S. De Tito, R. Romagnoli, B. Pagano, V. Limongelli, C. Giancola, P.G. Baraldi, L. Mayol, E. Novellino, A. Randazzo, J. Am. Chem. Soc. 132 (2010) 6425.
[31] S. Mulliri, A. Laaksonen, P. Spanu, R. Farris, M. Farci, F. Mingoia, G.N. Roviello, F. Mocci, Int. J. Mol. Sci. 22 (2021) 6028.

[32] M.A. Fik-Jaskółka, A.F. Mkrtchyan, A.S. Saghyan, R. Palumbo, A. Belter, L. A. Hayriyan, H. Simonyan, V. Roviello, G.N. Roviello, Spectrochim. Acta A Mol. Biomol. Spectrosc. 229 (2020) 117884.
[33] (a) P.L. Scognamiglio, C. Riccardi, R. Palumbo, T.F. Gale, D. Musumeci, G. N. Roviello, J. Nanostruct. Chem. (2023);
(b) V. Roviello, D. Musumeci, A. Mokhir, G.N. Roviello, Curr Med Chem. 28 (2021) 5004.
[34] (a) R. Galindo-Murillo, D.R. Roe, T.E. Cheatham, Biochim. Biophys. Acta (BBA) – Gen. Subjects 1850 (2015) 1041;
(b) S. Vangaveti, S.V. Ranganathan, A.A. Chen, WIREs RNA 8 (2016);
(c) I. Autiero, M. Saviano, E. Langella, Phys. Chem. Chem. Phys. 16 (2014) 1868.